Original article

Nuclear Medicine Communications

Efficacy of voxel-based dosimetry map for predicting response to trans-arterial radioembolization therapy for hepatocellular carcinoma: a pilot study

Min Young Yoo[a], Jin Chul Paeng[b], Hyo-Cheol Kim[c], Min Sun Lee[b,d,e], Jae Sung Lee[b,d,f], Dong Soo Lee[b,g], Keon Wook Kang[b,h] and Gi Jeong Cheon[b,h]

Objective **Typical clinical dosimetry models for trans-arterial radioembolization (TARE) assume uniform dose distribution in each tissue compartment. We performed simple voxel-based dosimetry using post-treatment ^{90}Y PET following TARE with ^{90}Y-resin microspheres and investigated its prognostic value in a pilot cohort.**

Method **Ten patients with 14 hepatocellular carcinoma lesions who underwent TARE with ^{90}Y-resin microspheres were retrospectively included. The partition model-based expected target tumor dose (TDp) was calculated using a pretreatment ^{99m}Tc-macroaggregated albumin scan. From post-treatment ^{90}Y-microsphere PET and voxel-wise S-value kernels, voxel-based dose maps were produced and the absorbed dose of each lesion (TDv) was calculated. Heterogeneity of intratumoral absorbed doses was assessed using the SD and coefficient of variation of voxel doses. The response of each lesion was determined based on contrast-enhanced MRI or CT, or both. Lesion responses were classified as local control success or failure. Prognostic values of dosimetry parameters and clinicopathological factors were evaluated in terms of progression-free survival (PFS) of each lesion.**

Results **TDv was significantly different between local control success and failure groups, whereas tumor size, TDp and intratumoral dose heterogeneity were not. Univariate survival analysis identified serum aspartate transaminase level ≥40 IU/L, tumor size ≥66 mm and TDv <81 Gy as significant prognostic factors for PFS. However, only TDv was an independent predictive factor in the multivariate analysis (P=0.022). There was a significant correlation between TDv and PFS (P=0.009; r=0.669).**

Conclusions **In TARE, voxel-based dose index TDv can be estimated on post-treatment ^{90}Y PET using a simple method. TDv was a more effective prognostic factor for TARE than TDp and clinicopathologic factors in this pilot study. Further studies are warranted on the role of voxel-based dose and dose distribution in TARE. *Nucl Med Commun* XXX: 000–000**

Nuclear Medicine Communications XXX, **XXX**:000–000

Keywords: **^{90}Y-microspheres, hepatocellular carcinoma, prognosis, radioembolization, voxel S values**

[a]Departments of Nuclear Medicine, Chungbuk National University Hospital, Cheongju, [b]Department of Nuclear Medicine, Seoul National University Hospital, [c]Department of Radiology, Seoul National University Hospital, [d]Interdisciplinary Program in Radiation Applied Life Science, Seoul National University, Seoul, [e]Nuclear Emergency and Environmental Protection Division, Korea Atomic Energy Research Institute, Daejeon, [f]Department of Biomedical Sciences, Seoul National University College of Medicine, [g]Department of Molecular Medicine and Biopharmaceutical Sciences, Graduate School of Convergence Science and Technology, Seoul National University, Seoul and [h]Cancer Research Institute, Seoul National University College of Medicine, Seoul, Republic of Korea

Correspondence to Jin Chul Paeng, MD, PhD, Department of Nuclear Medicine, Seoul National University Hospital, 101 Daehak-ro, Jongno-gu, Seoul 110-744, Korea
Tel: +82 2 2072 3341; fax: +82 2 745 7690; e-mail: paengjc@snu.ac.kr

Received 14 April 2021 **Accepted** 16 July 2021

Introduction

Hepatocellular carcinoma (HCC) is a highly lethal malignancy that is prevalent worldwide [1]. Among the treatment options for HCC, complete resection and liver transplantation are the only curative treatments. Trans-arterial radioembolization (TARE) is currently used as a bridging treatment or local control method for patients with intermediate-risk or advanced HCC who are not eligible for curative treatment [2,3]. TARE has shown better survival outcomes than other treatment options, such as trans-arterial chemoembolization and systemic chemotherapy, including sorafenib [4]. However, local control failure (LCF) is observed in approximately 20–50% of cases [4,5], probably because an insufficient radiation dose is supplied to tumor cells.

Pretreatment dose estimation can be performed using partition model dosimetry in a ^{99m}Tc-macroaggregated albumin (MAA) scan [6]. This method can estimate the mean absorbed radiation doses of tumors, normal liver tissues supplied by tumor-feeding arteries (in-target normal liver) and normal liver tissues supplied by nontumor-feeding arteries (out-target normal liver), assuming a uniform dose distribution in each tissue compartment

Supplemental Digital Content is available for this article. Direct URL citations appear in the printed text and are provided in the HTML and PDF versions of this article on the journal's website, www.nuclearmedicinecomm.com.

0143-3636 Copyright © 2021 Wolters Kluwer Health, Inc. All rights reserved.

DOI: 10.1097/MNM.0000000000001471

[7,8]. However, there may be considerable intratumoral heterogeneity in the actual dose distribution depending on various factors, including vessel density, thrombosis and tumor necrosis. Hence, intratumoral dose heterogeneity is considered an underlying cause of LCF [9].

Post-treatment bremsstrahlung single-photon emission computed tomography (SPECT)/computed tomography (CT) or PET/CT for ^{90}Y-microsphere is used for treatment verification after TARE [10], because they can show the real distribution of radioactivity. Additionally, voxel-based dosimetry using post-treatment ^{90}Y SPECT/CT or ^{90}Y PET/CT has been developed as a method to investigate the issue of intratumoral dose heterogeneity. Kafrouni *et al*., [11] demonstrated the correlation between treatment response and mean absorbed dose of tumors derived from voxel-based dosimetry based on post-treatment ^{90}Y PET.

In this study, voxel-based dosimetry was performed for each mass lesion using post-treatment ^{90}Y PET in patients who underwent TARE for HCC. This study aimed to investigate the prognostic values of radiation dose and intratumoral heterogeneity parameters obtained from voxel-based dosimetry and other clinical factors such as age, liver enzymes and tumor markers, in predicting the treatment outcomes of TARE.

Methods

Patients

This study retrospectively reviewed patients who underwent TARE with ^{90}Y-resin microspheres between July 2012 and September 2014. During the study period, 13 patients with HCC underwent TARE at our institution. Among them, 10 patients (all men; age, 59 ± 10 years; range, 48–84 years) were included and analyzed based on the following inclusion criteria: (1) confirmed HCC diagnosis, (2) presence of post-TARE ^{90}Y-microsphere PET data and (3) presence of follow-up records and imaging studies for evaluating treatment response. The clinicopathological information of each patient was obtained by reviewing their electronic medical records. The Institutional Review Board of Seoul National University Hospital approved the study design and waived the requirement for informed consent (H-2009-114-1158).

Trans-arterial radioembolization and PET image acquisition

TARE was performed as previously described [12]. During angiography planning, 185 MBq of ^{99m}Tc-MAA was injected into the tumor-feeding artery. Subsequently, a planar scan and SPECT/CT were performed to calculate the liver-to-lung shunt fraction (LSF) and the absorbed dose of normal organs (normal liver and lungs) and tumors. TARE was performed when the LSF on the planar scan was <20%. The dose of injected radioactivity was determined using the partition model method based on ^{99m}Tc-MAA SPECT/CT according to previous studies [6,7], with a target tumor dose of >120 Gy. TARE was performed by a single experienced interventional radiologist (H.C.K.) using ^{90}Y-labeled resin microspheres (SIR-Spheres; Sirtex Medical Ltd., Lane Cove, Australia). Radioactivity was adjusted, if necessary, according to the patient's condition and the operator's decision. The expected target tumor dose based on the partition model method (TDp) was calculated considering the adjusted administered dose [6]. ^{90}Y-microsphere PET/CT was performed using a large field-of-view PET/CT scanner (Biograph mCT64, Siemens Healthineers, Germany; axial field-of-view, 216 mm) immediately after TARE. CT images were acquired first (slice thickness, 5 mm; pitch, 1.2; 120 kVp, and 35 mAs) for attenuation correction and lesion localization. PET images were acquired using the 3D mode for one-bed position to cover the lower chest and upper abdomen for 10 min. The images were reconstructed on 200 × 200 matrices with a voxel size of 4.07 × 4.07 × 5 mm using an iterative method (2 iterations, 21 subsets) with an algorithm for point-spread function recovery and time-of-flight estimation, and a 5-mm Gaussian post-filter was applied.

Voxel-based dosimetry

The voxel S-value (VSV) kernel (Gy/MBq·s) convolution approach was used, where the VSV is a voxel-level medical internal radiation dose (MIRD) schema, defined as the mean absorbed dose in a target voxel per radioactive decay in a source voxel [13]. The voxel dose (D) was calculated by convolving the cumulated activity ($\tilde{A}$) with the VSV using the following equation:

$$D = \tilde{A} * VSV = \sum_{i=0}^{n} \tilde{A}_{voxel_i} \cdot VSV\left(voxel_j \leftarrow voxel_i\right)$$

VSV convolution was conducted using the VSV kernel reported in a free public database from Lanconelli *et al*., [14]. The VSV kernel of ^{90}Y generated in a soft tissue environment with a matrix size of 6 × 6 × 6 and voxel size of 3 × 3 × 3 mm was used. The PET images were resized such that their voxel size was the same as that of the VSV kernel. Accumulated activity maps were generated from the resized PET images by calculating the time-integrated activity from the injected time point to infinity, by using the physical half-life [15]. The 3D cumulated activity maps (MBq·s) were convoluted with the 3D VSV (Gy/MBq·s) to yield absorbed dose maps (Gy) using MATLAB software.

These absorbed dose maps were fused with contrast-enhanced MRI or CT images obtained immediately before TARE using a vendor-supplied software package (Syngo.via, Siemens Healthineers, Germany). The regions of interest for a tumor were drawn manually based on enhanced MRI or CT images on every image slice, and the volume-of-interest (VOI) for a tumor was

obtained by stacking all the tumor regions. From the VOI on the voxel-based dose map, the mean (TDv), SD and coefficient of variation of the absorbed dose distributions were measured for each tumor. Tumors smaller than 1 cm were excluded because of possible partial volume effects. A representative image of the tumor VOI is shown in Fig. 1.

Response evaluation and statistical analysis

The tumor response was determined based on follow-up imaging studies, including contrast-enhanced MRI or CT, or both. The local response of each lesion was determined according to the modified Response Evaluation Criteria in Solid Tumors criteria based on the European Association for the Study of the Liver guidelines [16–18]. Complete remission was defined as local control success (LCS), with other responses defined as LCF. Progression was analyzed for each lesion, and progression-free survival (PFS) was defined as the time from the date of TARE to the date of the imaging study that showed local control failure or progression.

Values are expressed as mean ± SD. The median values of the longest diameter, TDp and TDv of each tumor were used as cutoff values for survival analysis. For laboratory data [aspartate transaminase (AST), alanine transaminase and total bilirubin], the upper normal limit of each variable was used as the cutoff value. Univariate and multivariate survival analyses were performed using the Kaplan–Meier method and Cox regression analysis, respectively. Variables that were $P < 0.05$ in the univariate analysis were included in the multivariate analysis. The hazard ratio and 95% confidence interval (CI) were also calculated. Group comparisons of values (size, TDp, TDv and SD, and coefficient of variation of dose distribution in dose map) were performed using the Mann–Whitney U test. SD and coefficient of variation were used as heterogeneity indices in the VOI. Correlations between factors were assessed using Spearman's correlation analysis. *P* values less than 0.05 were considered statistically significant.

Results

Patients and treatment responses

During the study period, 13 patients with HCC underwent TARE at our institution. Among them, two patients were excluded because they were transferred to other hospitals and lost from follow-up, and one was excluded due to lack of post-TARE ^{90}Y PET. Finally, 10 patients (all men; age, 59 ± 10 years; range, 48–84 years) met the inclusion criteria and were included analysis. The patient characteristics are summarized in Table 1. No severe procedure-related complications after TARE were reported in any of the patients. The analysis included a total of 14 measurable lesions from the 10 patients, as 4 patients

Fig. 1

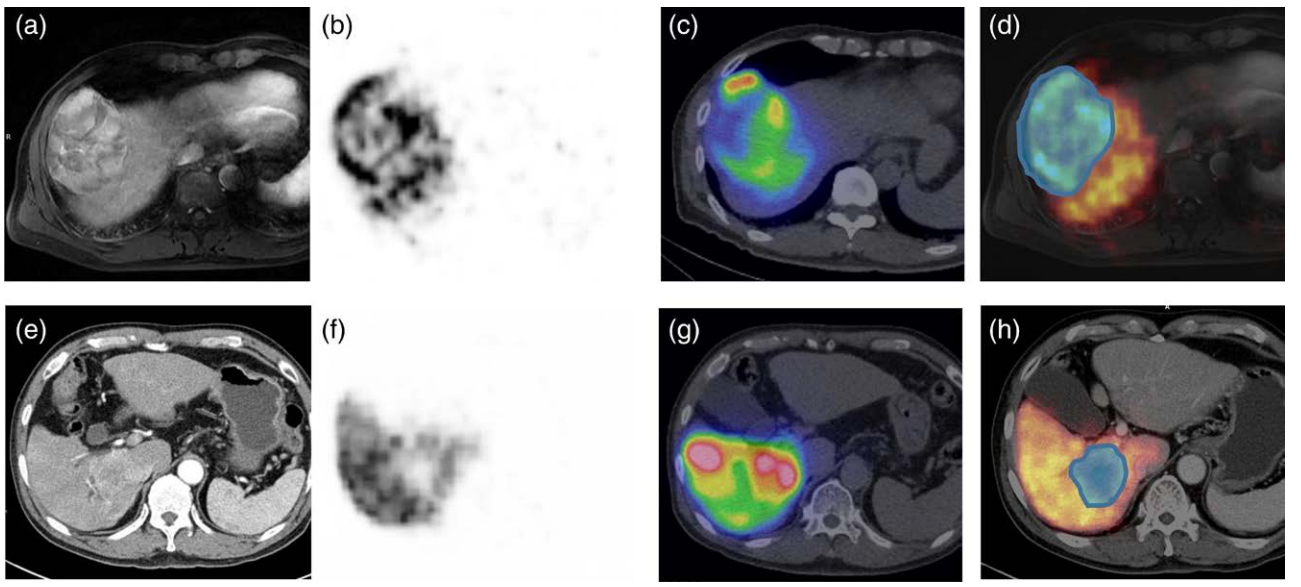

Representative images of patients showing local control success (top rows) and local control failure (bottom rows). In one patient, MRI showed a 92.3-mm-sized tumor (a) and the dose map obtained using ^{90}Y PET showed the absorption of a high dose, particularly in the tumor margin (b), which was a similar pattern to that seen on pretreatment ^{99m}Tc- macroaggregated albumin (MAA) single-photon emission computed tomography/computed tomography (c). Tumor volume-of-interest drawn on the fusion image of the dose map and MRI (d) showed a mean absorbed tumor dose (TDv) of 122.6 Gy, and the patient demonstrated a progression-free survival (PFS) of 29.5 months. In another patient (e), the dose map showed the absorption of a low dose in the tumor (f) in contrast to intense uptake on pretreatment ^{99m}Tc-MAA/CT (g) and a TDv of only 54.9 Gy (h). The patient's PFS was 1.5 months.

Table 1 Patient characteristics

Variables		Values (range)
Age, years		56 (48–84)[a]
Sex	Male	10
	Female	0
Baseline AFP (ng/mL)		359.5 (1.6–123000)[a]
Baseline PIVKA-II (mAU/mL)		1621.0 (21.0–75000)[a]
Child-Pugh class	A	9
	B	1
Viral status	HBV	7
	HCV	1
	NBNC	2
ECOG status	0	10
Portal vein thrombosis	Presence	6
	Absence	4
BCLC staging	Stage B	4
	Stage C	6

AFP, alpha-fetoprotein; BCLC staging, Barcelona Clinic Liver Cancer Staging; ECOG status, Eastern Cooperative Oncology Group performance status; HBV, hepatitis B virus; HCV, hepatitis C virus; NBNC, patients with neither hepatitis B nor hepatitis C; PIVKA-II, protein induced by vitamin K absence or antagonist-II.
[a]Median value (range).

Fig. 2

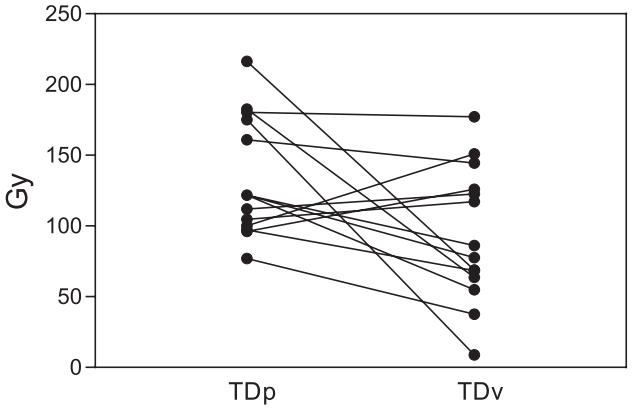

Case by case dosimetry for each tumor according to partition model-based dosimetry based on pretreatment ^{99m}Tc- macroaggregated albumin single-photon emission computed tomography (TDp) and according to voxel-based dosimetry based on post-treatment ^{90}Y-microsphere PET (TDv). TDp, expected target tumor dose; TDv, mean absorbed tumor dose.

had 2 lesions each. The average longest diameter of the tumors was 71.0 ± 40.7 mm.

Treatment response and voxel-based dosimetry

The median follow-up duration was 25.3 months (range, 2.1–29.7 months). Among 14 lesions, LCS was achieved in five lesions (36%) for a median duration of 25.6 months (range, 21.9–29.7 months). LCF was observed in the other nine lesions (64.3%) after a median follow-up of 1.5 months (range, 1.0–4.4 months). Dose maps were successfully generated using VSV kernel convolution (Fig. 1).

The median and mean ± SD of the TDv (81.9 Gy and 93.2 ± 47.7 Gy, respectively) were lower than those of the TDp (121.7 Gy and 135.9 ± 43.5 Gy, respectively) (Fig. 2). The tumor size was larger in the LCF group than in the LCS group, but the difference was not statistically significant (83.7 ± 45.1 mm vs. 48.2 ± 26.7 mm, Fig. 3a) ($P = 0.266$). The mean TDp of the LCF group was higher than that of the LCS group (144.6 ± 47.1 vs. 116.3 ± 30.7 Gy, Fig. 3b), but the difference was not statistically significant ($P = 0.199$). The TDv was significantly higher in the LCS group (132.3 ± 13.1 Gy; range, 117.2–150.9 Gy) than that in the LCF group (71.5 ± 43.3 Gy; range, 8.8–177.2 Gy) (Fig. 3c, $P = 0.021$). There were no significant differences in the heterogeneity indices of absorbed doses between the two groups (SD: $P = 0.266$; coefficient of variation: $P = 1.000$) (Supplementary Figure 1, Supplemental digital content 1, *http://links.lww.com/NMC/A201*).

Voxel-based dosimetry and survival

Univariate survival analyses conducted by including tumor factors and clinicopathological factors showed that high serum AST levels (≥40 IU/L), large tumor size (≥66 mm) and low TDv (<81 Gy) were significant prognostic factors for poor PFS ($P = 0.019$, 0.042 and 0.026, respectively; Table 2). The cutoff values for tumor size and TDv were 66 and 81 Gy, respectively. In the univariate analysis of TDp performed using a cutoff value of 121.7 Gy (median value), TDp was not statistically significant for prognosis. Kaplan–Meier survival curves for these factors are shown in Fig. 4. Multivariate analysis including these factors identified only TDv as an independent predictive factor for PFS ($P = 0.022$; hazard ratio, 21.018; 95% CI, 1.549–285.204). TDv and PFS were significantly correlated ($r = 0.669$, $P = 0.009$), and five of the six lesions (83%) with TDv ≥81 Gy had PFS >20 months (Fig. 5). In the analyses for overall survival, TDv was also selected as a significant prognostic factor in univariate analysis, although it was not in multivariate analysis (Supplementary Table 1, Supplemental digital content 2, *http://links.lww.com/NMC/A202*).

Discussion

In the present study, we applied a simple voxel-based dosimetry approach to a pilot cohort who underwent TARE using ^{90}Y-resin microspheres and demonstrated that the dose calculated for each lesion is effective for predicting outcomes.

In TARE, radiopharmaceuticals are directly injected into the tumor-feeding arteries and do not show redistribution after initial embolization. Thus, the calculation of the radiation dose in TARE is easier than that for other systemically administered radioactive drugs. Pretreatment planning angiography is currently performed using ^{99m}Tc-MAA, and many institutions perform a post-treatment scan to assess the results of TARE. Because ^{90}Y is a pure beta-emitter, post-treatment scans are performed using bremsstrahlung gamma images or PET images. Radiation dosimetry methods using bremsstrahlung images are also based on the MIRD schema [19,20], and

Fig. 3

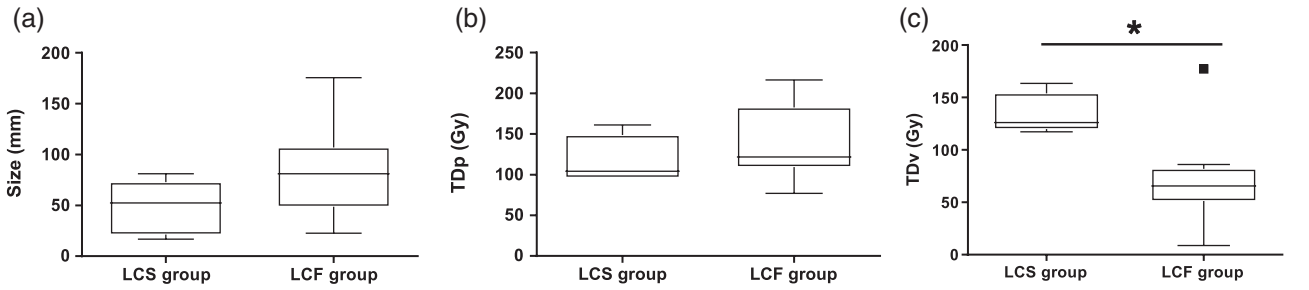

Box plots for TDp, tumor size and TDv according to treatment response. (a) Average tumor size and (b) TDp based on pretreatment ^{99m}Tc- macroaggregated albumin (MAA) single-photon emission computed tomography/computed tomography was not significantly different between the local control success (LCS) and local control failure (LCF) groups (P=0.266 and P=0.199). (c) However, TDv was significantly higher in the LCS group than in the LCF group (P=0.021). TDp, expected target tumor dose; TDv, mean absorbed tumor dose.

Table 2. Results of survival analysis for progression-free survival

	Univariate analysis		Multivariate analysis	
Variables	Hazard ratio (95% CI)	*P* value	Hazard ratio (95% CI)	*P* value
Age (years)		0.974		
<65	1.000			
≥65	1.026 (0.209–5.031)			
Portal vein thrombosis		0.301		
Absent	1.000			
Present	2.008 (0.495–8.155)			
Viral status		0.975		
HBV/HCV	1.000			
NBNC	1.026 (0.209–5.031)			
AST (IU/L)		0.019		0.289
<40	1.000			
≥40	5.367 (1.078–26.73)			
ALT (IU/L)		0.267		
<40	1.000			
≥40	2.034 (0.539–7.678)			
Total bilirubin (mg/dL)		0.267		
<1.2	1.000			
≥1.2	2.034 (0.539–7.678)			
Baseline AFP (ng/ml)		0.199		
<400	1.000			
≥400	0.426 (0.105–1.722)			
Baseline PIVKA-II		0.286		
<100	1.000			
≥100	24.085 (0.002–302104.1)			
Size (mm)		0.042		0.506
<66	1.00			
≥66	3.741 (0.915–15.29)			
TDp (Gy)		0.953		
<121.7	1.043 (0.260–4.186)			
≥121.7	1.000			
TDv (Gy)		0.026		0.022
<81	11.187 (1.341–93.34)		21.018 (1.549–285.2)	
≥81	1.000		1.000	

AFP, alpha-fetoprotein; ALT, alanine transaminase; AST, aspartate transaminase; CI, confidence interval; HBV, hepatitis B virus; HCV, hepatitis C virus; NBNC, patients with neither hepatitis B nor hepatitis C; PIVKA-II, protein induced by vitamin K absence or antagonist-II; TDp, absorbed dose based on partition model; TDv, absorbed dose based on dose map.

Gulec *et al*., [21] reported the use of this schema for the dosimetry of ^{90}Y-microspheres confined to the liver. The usual MIRD schema assumes a uniform distribution of radioactivity in a certain organ or tissue. However, in the real world, therapeutic radiopharmaceuticals show heterogeneous distributions in target tissues or organs because of vasculature heterogeneity, anatomical variation and tissue necrosis.

The present study adopted voxel-based dosimetry, in which the intratumoral heterogeneity of ^{90}Y-microsphere distribution was considered [22]. In this voxel-based dosimetry approach, the ^{90}Y-VSV was convoluted with the PET cumulative activity map at the voxel level to create a voxel-based absorbed dose map. This is an easier approach than those using patient-specific Monte Carlo simulations and has shown accurate dosimetry results in

Fig. 4

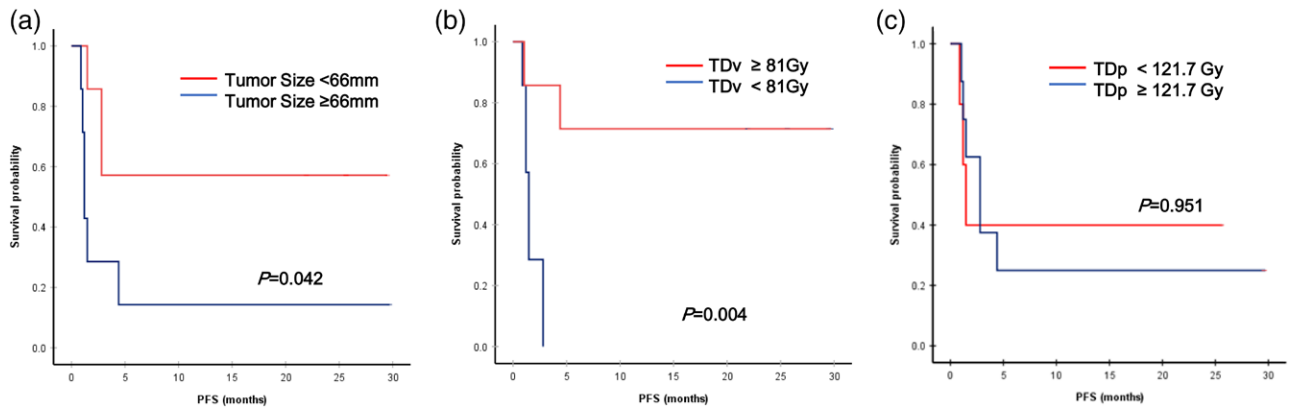

Kaplan–Meier survival curves showing significant differences in progression-free survival (PFS) according to tumor size (a) and TDv (b). However, TDp was not related to a significant difference in PFS (c). TDp, expected target tumor dose; TDv, mean absorbed tumor dose.

Fig. 5

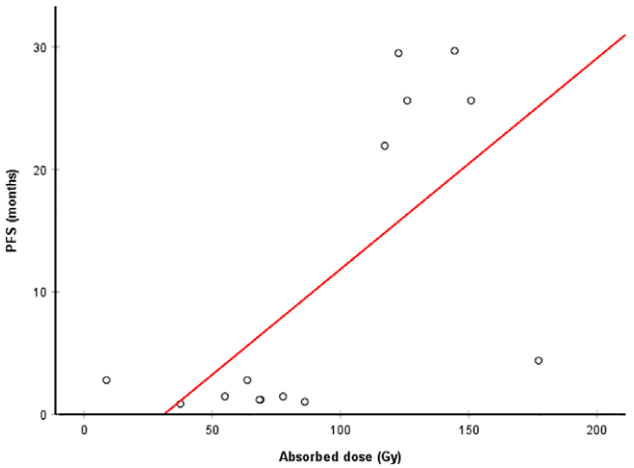

Correlation analysis for the relationship between mean absorbed tumor dose (TDv) and progression-free survival (PFS); a significant correlation was observed (P=0.009, r=0.669).

uniform-density organs, such as the liver [23,24]. Based on the voxel-based dose map, the TDv of each lesion was successfully calculated. Despite the TDp planned based on the pretreatment scan, there was considerable variation in TDv, from 40 Gy to 177 Gy, which may be one of the main reasons for the difference in treatment outcomes. While small tumor size, low AST levels and higher TDv (median, ≥81 Gy) were significant prognostic factors for successful treatment in univariate analyses, the multivariate analysis confirmed TDv as the only independent prognostic factor. Previous studies have reported clinical factors related to hepatic function (total bilirubin and albumin) and tumor aggressiveness (alpha-fetoprotein level, portal vein thrombosis and tumor size) as significant prognostic factors in patients treated with TARE [25,26]. In our study, these factors were NS, probably because of the small sample size. Further studies with a larger cohort are needed to determine the role of these factors.

When applying partition model to pretreatment simulation scans, 120 Gy has been deemed a target dose for effective treatment. In this study, the median TDp using pretreatment ^{99m}Tc-MAA SPECT/CT was estimated to be 121.7. However, the post-treatment absorbed dose of the TDv was different from the pretreatment assumption. The causes of such different dose calculations could include differences in the in-vivo distribution of particles (^{99m}Tc-MAA *vs.* ^{90}Y-microspheres) according to differences in catheter tip location, flow dynamics, number of particles and change in perfused volumes [27]. We observed an obvious difference in PFS between groups showing high and low absorbed doses of TDv, which was not observed for TDp. Consistent with previously published data, TDv based on post-treatment ^{90}Y-microsphere PET is more significantly correlated with prognosis than TDp [28–30]. In Fig. 4, the cutoff of the TDv was set at 80–120 Gy, and we also observed a significant correlation between TDv and PFS.

Because we performed voxel-based dosimetry, it was possible to evaluate voxel-wise intratumoral heterogeneity. High intratumoral heterogeneity has been assumed to be related to LCF, even when a high average dose is delivered to a tumor. The SD and coefficient of variation of dose distributions in a tumor were measured as simple indices for heterogeneity [31]. Although there was no significant difference in these values between the LCS and LCF groups in our study, further studies including a larger number of cases are warranted to investigate the effects of intratumoral dose heterogeneity. As shown in this study, TDv can be an effective prognostic factor in TARE based on the accurate estimation of radiation dose

and dose distribution. TDv could help early determination of treatment efficacy, and need of adjuvant therapy in case of suboptimal treatment. Furthermore, TDv could also be helpful for selecting appropriate treatment candidates and well-tolerated doses [32].

This study has several limitations. First, only a small number of patients with inoperable HCC who underwent a single TARE session with ^{90}Y-resin microspheres were included because this was a pilot study. Although voxel-based dosimetry is effective for predicting outcomes, its efficacy needs to be compared with conventional dosimetry methods. Further studies with larger cohorts are required to investigate the role of voxel-based dosimetry in clinical practice. Second, we used only simple indices for intratumoral heterogeneity. Other indices of dose heterogeneity must be investigated.

Conclusion

In TARE using a ^{90}Y-microsphere, the voxel-wise absorbed dose can be easily estimated using post-treatment ^{90}Y PET with a simple voxel-based dosimetry method conducted using VSV kernels. The TDv calculated by voxel-based dosimetry is a significant prognostic factor for the outcome of TARE using ^{90}Y-resin microspheres in patients with HCC, with a cutoff value of 80–120 Gy. Further studies are required to determine the roles of tumor dose and intratumoral heterogeneity in the treatment response.

Acknowledgements

This study was reviewed and approved by the Institutional Review Board of Seoul National University Hospital. The requirement for written informed consent was waived because of the retrospective nature of the study (H-2009-114-1158).

This work was supported by a grant from the National Research Foundation of Korea (NRF) funded by the Korean Ministry of Science and ICT (NRF-2020M2D9A109398911).

J.C.P., J.S.L., M.S.L. and M.Y.Y. designed the study and drafted the manuscript. J.S.L., M.S.L. and M.Y.Y. performed the analyses and interpreted the results. J.C.P. and J.S.L. have revised the manuscript. H.C.K., K.W.K., D.S.L. and G.J.C. collected the clinical data. All authors read and approved the final manuscript.

Conflicts of interest

There are no conflicts of interest.

References

1 El-Serag HB, Rudolph KL. Hepatocellular carcinoma: epidemiology and molecular carcinogenesis. *Gastroenterology* 2007; **132**:2557–2576.
2 Jelic S, Sotiropoulos GC; ESMO Guidelines Working Group. Hepatocellular carcinoma: ESMO clinical practice guidelines for diagnosis, treatment and follow-up. *Ann Oncol* 2010; **21** (Suppl 5):v59–v64.
3 Thomas MB, Jaffe D, Choti MM, Belghiti J, Curley S, Fong Y, *et al*. Hepatocellular carcinoma: consensus recommendations of the National Cancer Institute Clinical Trials Planning Meeting. *J Clin Oncol* 2010; **28**:3994–4005.
4 Moreno-Luna LE, Yang JD, Sanchez W, Paz-Fumagalli R, Harnois DM, Mettler TA, *et al*. Efficacy and safety of transarterial radioembolization versus chemoembolization in patients with hepatocellular carcinoma. *Cardiovasc Intervent Radiol* 2013; **36**:714–723.
5 Lewandowski RJ, Kulik LM, Riaz A, Senthilnathan S, Mulcahy MF, Ryu RK, *et al*. A comparative analysis of transarterial downstaging for hepatocellular carcinoma: chemoembolization versus radioembolization. *Am J Transplant* 2009; **9**:1920–1928.
6 Ho S, Lau WY, Leung TW, Chan M, Ngar YK, Johnson PJ, Li AK. Partition model for estimating radiation doses from yttrium-90 microspheres in treating hepatic tumours. *Eur J Nucl Med* 1996; **23**:947–952.
7 Dezarn WA, Cessna JT, DeWerd LA, Feng W, Gates VL, Halama J, *et al*.; American Association of Physicists in Medicine. Recommendations of the American Association of Physicists in Medicine on dosimetry, imaging, and quality assurance procedures for 90Y microsphere brachytherapy in the treatment of hepatic malignancies. *Med Phys* 2011; **38**:4824–4845.
8 Loevinger R, Budinger T, Watson E. *MIRD primer for absorbed dose calculations.* Revised ed. The Society of Nuclear Medicine, Inc.; 1991.
9 Sangro B, Iñarrairaegui M, Bilbao JI. Radioembolization for hepatocellular carcinoma. *J Hepatol* 2012; **56**:464–473.
10 Pasciak AS, Bourgeois AC, Bradley YC. A Comparison of techniques for (90)Y PET/CT image-based dosimetry following radioembolization with resin microspheres. *Front Oncol* 2014; **4**:121.
11 Kafrouni M, Allimant C, Fourcade M, Vauclin S, Delicque J, Ilonca AD, *et al*. Retrospective voxel-based dosimetry for assessing the ability of the body-surface-area model to predict delivered dose and radioembolization outcome. *J Nucl Med* 2018; **59**:1289–1295.
12 Song YS, Paeng JC, Kim HC, Chung JW, Cheon GJ, Chung JK, *et al*. PET/CT-based dosimetry in 90Y-microsphere selective internal radiation therapy: single cohort comparison with pretreatment planning on 99mTc-MAA imaging and correlation with treatment efficacy. *Medicine* 2015; **94**:23.
13 Bolch WE, Bouchet LG, Robertson JS, Wessels BW, Siegel JA, Howell RW, *et al*. MIRD pamphlet No. 17: the dosimetry of nonuniform activity distributions–radionuclide S values at the voxel level. Medical Internal Radiation Dose Committee. *J Nucl Med* 1999; **40**:11S–36S.
14 Lanconelli N, Pacilio M, Lo Meo S, Botta F, Di Dia A, Aroche AT, *et al*. A free database of radionuclide voxel S values for the dosimetry of nonuniform activity distributions. *Phys Med Biol* 2012; **57**:517–533.
15 Cremonesi M, Chiesa C, Strigari L, Ferrari M, Botta F, Guerriero F, *et al*. Radioembolization of hepatic lesions from a radiobiology and dosimetric perspective. *Front Oncol* 2014; **4**:210.
16 Bruix J, Sherman M, Llovet JM, Beaugrand M, Lencioni R, Burroughs AK, *et al*.; EASL Panel of Experts on HCC. Clinical management of hepatocellular carcinoma. Conclusions of the Barcelona-2000 EASL conference. European Association for the Study of the Liver. *J Hepatol* 2001; **35**:421–430.
17 Gillmore R, Stuart S, Kirkwood A, Hameeduddin A, Woodward N, Burroughs AK, Meyer T. EASL and mRECIST responses are independent prognostic factors for survival in hepatocellular cancer patients treated with transarterial embolization. *J Hepatol* 2011; **55**:1309–1316.
18 Lencioni R, Llovet JM. Modified RECIST (mRECIST) assessment for hepatocellular carcinoma. *Semin Liver Dis* 2010; **30**:52–60.
19 Siegel JA, Zeiger LS, Order SE, Wallner PE. Quantitative bremsstrahlung single photon emission computed tomographic imaging: use for volume, activity, and absorbed dose calculations. *Int J Radiat Oncol Biol Phys* 1995; **31**:953–958.
20 Siegel J, Handy D, Kopher K, Zeiger L, Order S. Therapeutic beta irradiating isotopes in bony metastasis: a technique for bremsstrahlung imaging and quantitation. *Antibody Immunoconj Radiopharm* 1992; **5**:237–248.
21 Gulec SA, Mesoloras G, Stabin M. Dosimetric techniques in 90Y-microsphere therapy of liver cancer: the MIRD equations for dose calculations. *J Nucl Med* 2006; **47**:1209–1211.
22 Dieudonné A, Hobbs RF, Bolch WE, Sgouros G, Gardin I. Fine-resolution voxel S values for constructing absorbed dose distributions at variable voxel size. *J Nucl Med* 2010; **51**:1600–1607.
23 Levillain H, Duran Derijckere I, Marin G, Guiot T, Vouche M, Reynaert N, *et al*. 90Y-PET/CT-based dosimetry after selective internal radiation therapy predicts outcome in patients with liver metastases from colorectal cancer. *EJNMMI Res* 2018; **8**:60.
24 Allimant C, Kafrouni M, Delicque J, Ilonca D, Cassinotto C, Assenat E, *et al*. Tumor targeting and three-dimensional voxel-based dosimetry to predict tumor response, toxicity, and survival after yttrium-90 resin microsphere

radioembolization in hepatocellular carcinoma. *J Vasc Interv Radiol* 2018; **29**:1662–1670.e4.
25 Bauschke A, Altendorf-Hofmann A, Freesmeyer M, Winkens T, Malessa C, Schierz JH, *et al*. [Selective internal radioembolization in nonresectable hepatocellular carcinoma]. *Chirurg* 2016; **87**:956–963.
26 Jeliazkova P, Umgelter A, Braren R, Kaissis G, Mustafa M, Einwächter H. Prognostic factors in hepatocellular carcinoma patients undergoing transarterial chemoembolization and radioembolization: a retrospective study. *Eur J Gastroenterol Hepatol* 2020; **32**:1036–1041.
27 Thomas MA, Mahvash A, Abdelsalam M, Kaseb AO, Kappadath SC. Planning dosimetry for 90 Y radioembolization with glass microspheres: evaluating the fidelity of 99m Tc-MAA and partition model predictions. *Med Phys* 2020; **47**:5333–5342.
28 Chiesa C, Lambert B, Maccauro M, Ezziddin S, Ahmadzadehfar H, Dieudonné A, *et al*. Pretreatment dosimetry in HCC radioembolization with (90)Y glass microspheres cannot be invalidated with a bare visual evaluation of (99m)Tc-MAA uptake of colorectal metastases treated with resin microspheres. *J Nucl Med* 2014; **55**:1215–1216.
29 Wondergem M, Smits ML, Elschot M, de Jong HW, Verkooijen HM, van den Bosch MA, *et al*. 99mTc-macroaggregated albumin poorly predicts the intrahepatic distribution of 90Y resin microspheres in hepatic radioembolization. *J Nucl Med* 2013; **54**:1294–1301.
30 Garin E, Lenoir L, Edeline J, Laffont S, Mesbah H, Porée P, *et al*. Boosted selective internal radiation therapy with 90Y-loaded glass microspheres (B-SIRT) for hepatocellular carcinoma patients: a new personalized promising concept. *Eur J Nucl Med Mol Imaging* 2013; **40**:1057–1068.
31 Watabe T, Tatsumi M, Watabe H, Isohashi K, Kato H, Yanagawa M, *et al*. Intratumoral heterogeneity of F-18 FDG uptake differentiates between gastrointestinal stromal tumors and abdominal malignant lymphomas on PET/CT. *Ann Nucl Med* 2012; **26**:222–227.
32 Bastiaannet R, Kappadath SC, Kunnen B, Braat AJAT, Lam MGEH, de Jong HWAM. The physics of radioembolization. *EJNMMI Phys* 2018; **5**:22.